PAPERS IN PHYSICS, VOL. 18, ART. 180001 (2026)

www.papersinphysics.org

Received: 07 March 2025, Accepted: 08 November 2025
Edited by: Francisco Melo, Universidad de Santiago de Chile

DOI: https://doi.org/10.4279/PIP.170001

ISSN 1852-4249

Effect of sol-gel preparation on the microstructural and thermal behavior of nanosized powder of mesoporous hydroxyapatite

Jan Ady[1]*, Djony Izak Rudyardjo[1], Gunarti Meylinda Putri[1], Akhmad Arsyad Ulul Amri[1]

The effect of sol-gel preparation on the microstructural and thermal behavior of nanosized mesoporous hydroxyapatite powder was investigated in this study. The powder was synthesized using the sol-gel technique, with preparation carried out at various temperatures: room temperature 100°C and 400°C. FTIR analysis revealed the presence of hydroxyl groups (3423.91 cm^{-1} to 3600 cm^{-1}), corresponding to the stretching vibration of hydroxyl (OH) and phosphate ions (1102.31 cm^{-1} to 1644.17 cm^{-1}), indicating the stretching vibration of P - O, and these indicating the functional groups of PO_4^{3-}, confirmed as the formation of hydroxyapatite. The thermal properties were studied using DSC-TG and provide valuable information on phase transitions such as melting, crystallization, thermal enthalpy, and specific heat capacity. XRD analysis confirmed all materials as nanosized mesoporous hydroxyapatite powder with face-centered cubic unit cells in the hexagonal lattice system. The lattice constants were obtained, a = b = 0.942 nm and c = 0.588 nm; these results were determined by careful analysis using the appropriate interplanar spacing formula. Finally, the surface topology and elemental composition were examined using SEM-EDX, including the atomic ratio of elements in the nanosized mesoporous hydroxyapatite powder. The Ca/P ratios were found to be approximately 1.63 and 1.73 for samples treated at temperatures of 100°C and 400°C, respectively. In the future, nanosized mesoporous hydroxyapatite powder, synthesized by the sol-gel method, could be prepared as a raw material for waste adsorbents.

I Introduction

Hydroxyapatite is a member of the apatite family, featuring hydroxyl ions (OH^-) and phosphate ions (PO_4^{3-}). Hydroxyapatite (HAP) has the chemical formula $Ca_5(PO_4)_3(OH)$, although it is commonly written as $Ca_{10}(PO_4)_6(OH)_2$ [1–3]. In recent years, HAP has become the main component of natural bone. Therefore, it has been extensively investigated for medical applications due to its excellent biocompatibility and nontoxicity to human cells. Furthermore, HAP has excellent adsorption and filtration capabilities, making it suitable for use as an element or composite material for adsorbents, particularly for the adsorption of industrial and pharmaceutical waste [4–7]. HAP can be synthesized using various chemical methods, such as precipitation, hydrothermal, and sol-gel techniques. These methods are commonly used in the preparation of materials, particularly for the production of nanoparticles or various types of ceramics. However, this research focuses on sample preparation using the sol-gel technique [8–13], as this process operates at relatively low temperatures and allows fine control over the composition and structure of materials. The sol-gel process involves the transition of a solution (sol) into a gel-like network and is widely used to produce metal oxides or ceramics. In the sol-gel technique, the liquid phase (the sol) is typically prepared by dissolving a metal precursor, such as metal alkoxides or salts, in a solvent. The sol then undergoes hydrolysis and condensation reactions to form a gel which is subsequently dried and heat-treated to

* jan-a@fst.unair.ac.id

[1] University of Airlangga, 60115 Surabaya, Indonesia.

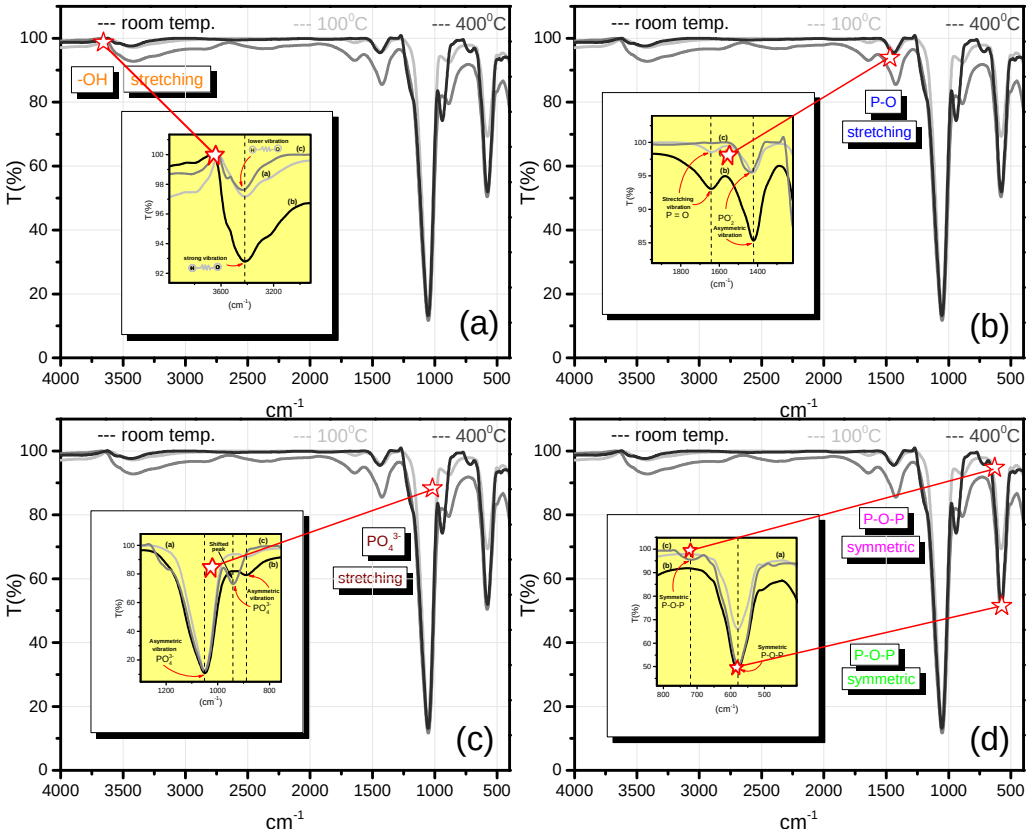

Figure 1: FTIR spectra of nanosized mesoporous hydroxyapatite powder

form solid materials. In this study, the synthesis of hydroxyapatite powder was performed using the sol-gel preparation technique. The powder was dried at various temperatures: room temperature, 100°C and 400°C, to form solid nanosized mesoporous hydroxyapatite. In this research, the effect of sol-gel preparation on the microstructural and thermal behavior of nanosized mesoporous hydroxyapatite powder was studied using data analysis from FTIR [14–16], DSC-TG [17–21], XRD [22–28] and SEM-EDX [29–35] test results.

II Materials and methods

Calcium hydroxide powders (Ca $(OH)_2$) and phosphoric acid powders (H_3PO_4), both with a purity of more than 90%, sourced from Merck, serve as primary precursors to synthesize nanosized mesoporous hydroxyapatite powders using the sol-gel preparation technique performed in this research. The high purity of these chemicals ensures that the formation of the nanosized mesoporous hydroxyapatite powder product is consistent and of high quality. In this process, calcium hydroxide provides the calcium source, while phosphoric acid supplies the phosphate component essential for forming nano-sized mesoporous hydroxyapatite powder. These two precursors are carefully mixed under controlled conditions for nine hours to initiate the sol-gel process, during which ethanol droplets (C_2H_5OH) are added to the solution throughout the hydrolysis and condensation process. The gel product is then aged for 24 hours at room temperature, followed by drying at 100°C and 400°C. Ultimately, nanosized mesoporous hydroxyapatite powder is obtained, a material that is being prepared as a mesoporous adsorbent, particularly for use as a raw material in waste adsorbents in ongoing research. FTIR analysis was performed to characterize the chemical bonds and functional groups present in the material, providing valuable insights into the molecular structure and vibrational modes of the functional groups of nano-sized mesoporous hydroxyapatite pow-

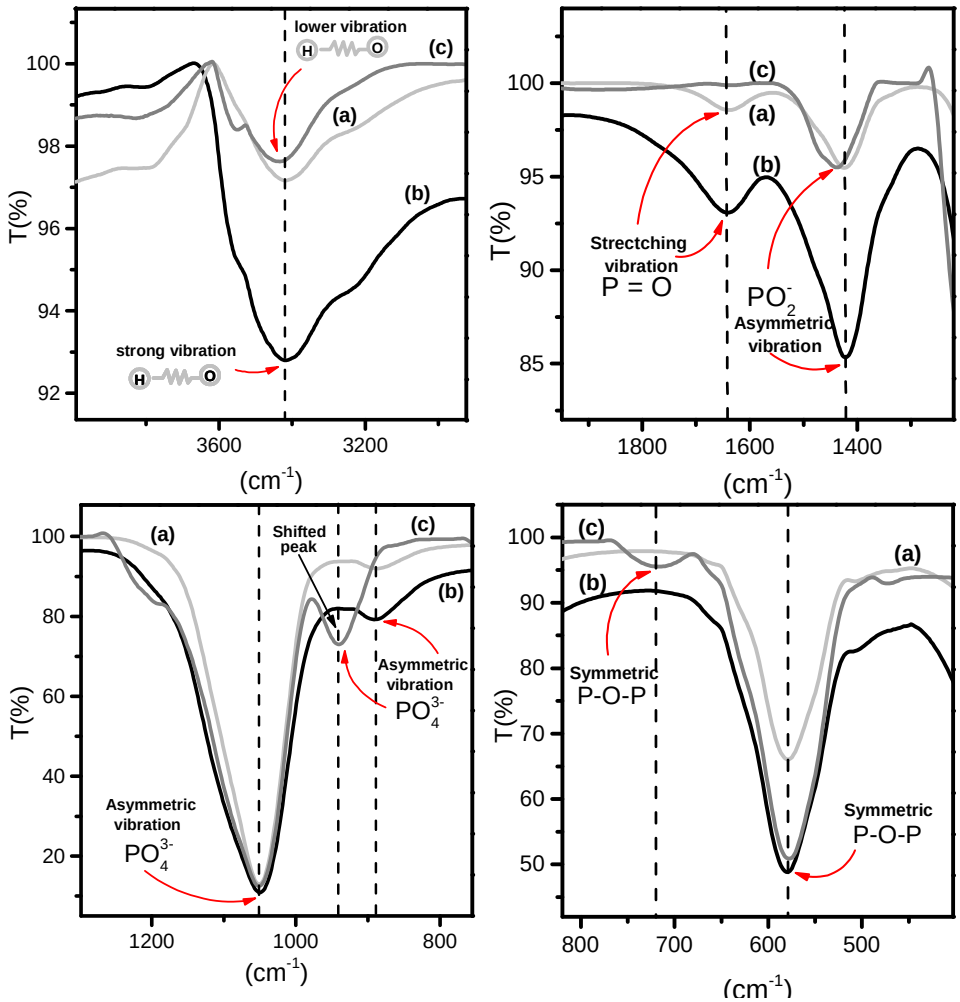

Figure 2: FTIR spectra of nanosized mesoporous hydroxyapatite powder in within specific wavenumber ranges at various temperatures; (a) room , (b) 100°C, and (c) 400°C

der. DSC-TG analysis was performed to obtain valuable information on phase transitions such as melting, crystallization, thermal enthalpy, and specific heat capacity. XRD analysis was conducted to determine the crystalline structure, including the hexagonal lattice system of mesoporous hydroxyapatite powder, and to determine the crystallite size. SEM-EDX was used to provide information on the surface topology and elemental composition, including the atomic ratio of elements in the nanosized mesoporous hydroxyapatite powder.

III Results and discussion

Several results and data have been obtained regarding the quantity of nanosized mesoporous hydroxyapatite powder prepared using the sol-gel technique. These results demonstrate the effects of different temperatures during synthesis, specifically at room temperature, 100°C, and 400°C.

i FTIR Results and discussions

Fourier Transform infrared (FTIR) spectroscopy revealed the presence of hydroxyl groups, with stretching vibrations occurring within the range of approxi-

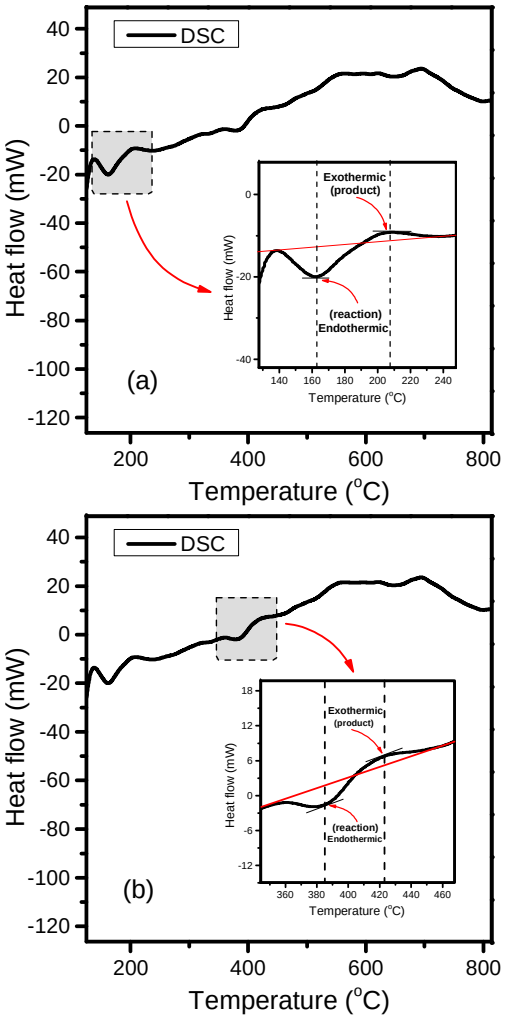

Figure 3: The DSC thermogram of nanosized mesoporous hydroxyapatite powder in the enthalpy of phase transition at various temperature ranges: (a) in the range 100°C – 229°C, and (b) in the range 350°C – 443°C.

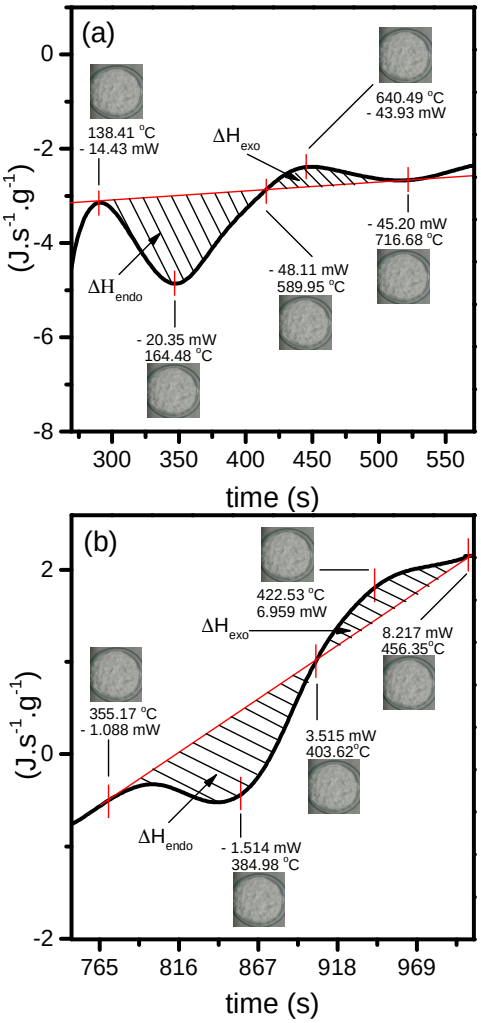

Figure 4: (a) and (b) Enthalpic transitions of fusion (ΔH_f) and crystallization (ΔH_c) of nano-sized mesoporous hydroxyapatite powder over specific time intervals.

mately 3423.91 cm^{-1} to 3601.21 cm^{-1}, corresponding to the –OH group. The strongest hydroxyl vibration was observed with a transmittance percentage of approximately 92.76% for nanosized mesoporous hydroxyapatite powder at 100°C. Meanwhile, weaker transmittance percentages were observed at 97.14% at room temperature and 97.65% at 400°C. The phosphorus oxide group was identified as P–O, with stretching vibrations occurring within the range of approximately 1102.31 cm^{-1} to 1644.17 cm^{-1}. The strongest stretching vibration for P-O occurred at 100°C, with a transmittance percentage of approximately 93.76%. The weakest transmittance percentages were 95.53% at room temperature and 99.24% at 400°C, respectively.

Symmetrical and asymmetric O-P-O vibrations were observed at different values of the stretching vibration frequencies, especially for samples prepared at 100°C. Lower vibration frequencies of stretching were observed for these nanosized mesoporous hydroxyapatite powders, which were prepared at room temperature and 400°C (see Fig. 1 and Fig. 2). These results confirm the presence of functional groups of nanosized mesoporous hydroxyapatite powders, which were pre-

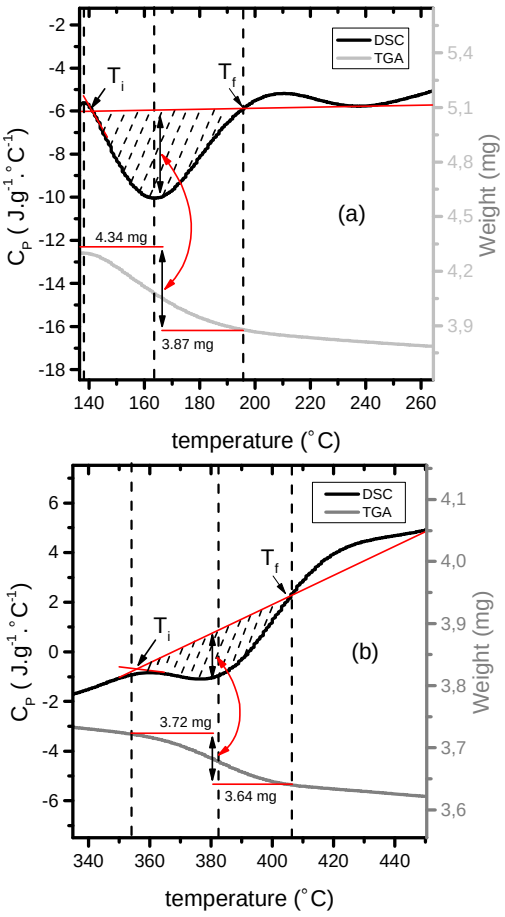

Figure 5: The specific heat capacity and weight analysis of the nano-sized mesoporous hydroxyapatite powder samples were performed at the following temperature ranges: (a) $T_i \approx 142.32\,^{\circ}C$ to $T_f \approx 233.87\,^{\circ}C$, and (b) $T_i \approx 361.04\,^{\circ}C$ to $T_f \approx 446.26\,^{\circ}C$.

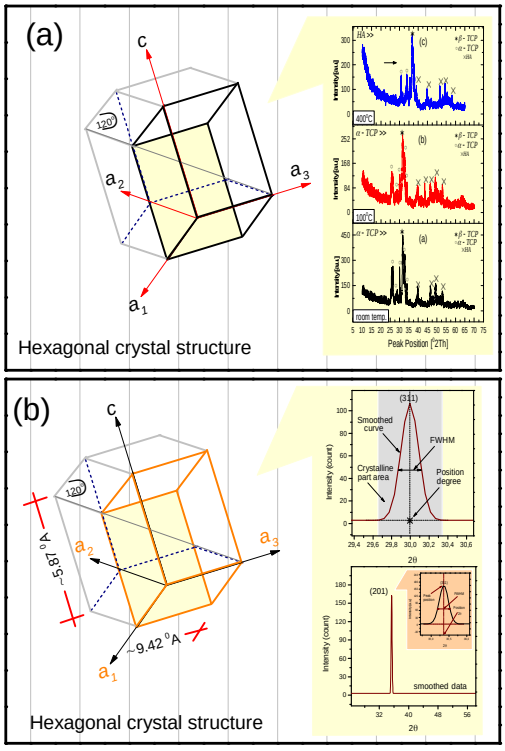

Figure 6: The hexagonal crystal structure of nano-sized mesoporous hydroxyapatite powder with lattice constants: $a_0 = b_0 \approx 9.416\,\text{Å}$ and $c_0 \approx 5.878\,\text{Å}$. (b) The refinement curve for FWHM and the peaks of the XRD pattern used to determine the lattice parameters.

pared using the sol-gel technique.

ii DSC-TG Results and discussions

The thermogram results of the gel-to-dry process of the nanosized mesoporous hydroxyapatite powder were examined using Differential Scanning Calorimetry (DSC) and Thermogravimetric Analysis (TG), with the temperature increasing from 27°C to 100°C. In the DSC curves, the plot shows the heat flow as a function of the temperature increase (see Fig. 3). These curves exhibit two distinct enthalpy transitions corresponding to exothermic and endothermic processes, as seen in the zoomed-in inserts (see Fig. 3). The fusion and crystallization enthalpies of the sample are calculated by integrating the peak areas, expressed in units of $\text{J.s}^{-1}.\text{g}^{-1}.\text{s}$ (see Fig. 4). Based on these DSC results, the preferred effective temperatures for the synthesis of powdered nanosized mesoporous hydroxyapatite are found to be at room temperature, 100°C and 400°C.

The fusion and crystallization enthalpies were determined, and these values are reported in Table 1. The specific heat capacity, also known as massic heat capacity, is a thermal property of the nanosized mesoporous hydroxyapatite powder. It is expressed in units of $\text{J}\cdot\text{g}^{-1}\cdot{}^{\circ}\text{C}^{-1}$. This property was measured to assess the thermal response as the composition changes with temperature and pressure. The initial (Ti) and final (Tf) temperatures for fusion and crystallization enthalpies were determined based on the specific heat capacity. Two distinct temperature ranges for melting or fusion were identified: one occurring from Ti = 143.24°C to Tf = 233.87°C, and the other from Ti = 361.04°C to

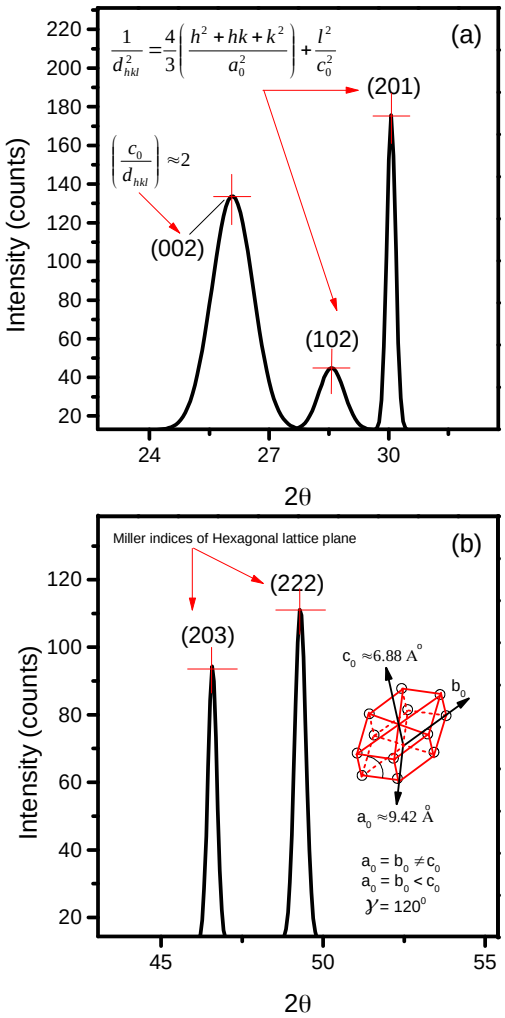

Figure 7: XRD patterns of nanosized mesoporous hydroxyapatite powder at 27°C by the Bragg's angle position in the intervals (a) 21° to 37° and (b) 48° to 54°.

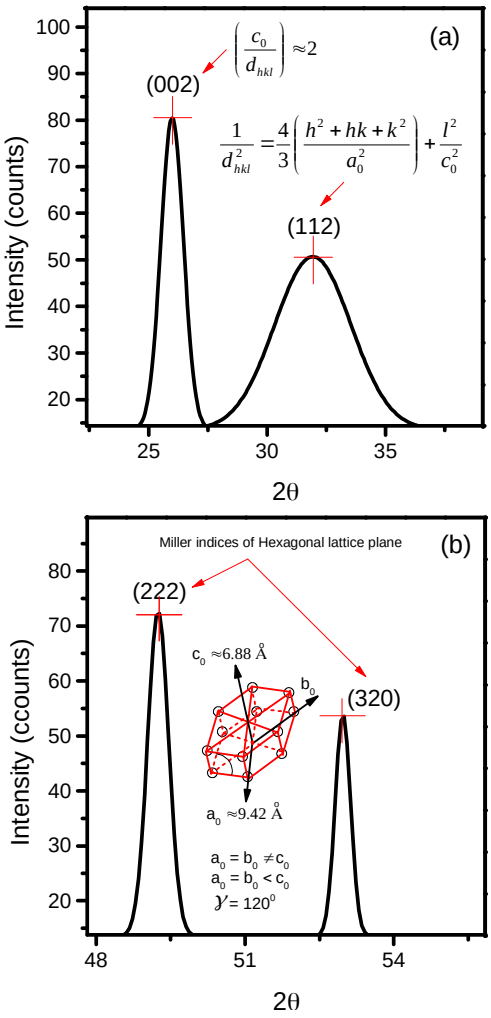

Figure 8: XRD patterns of nanosized mesoporous hydroxyapatite powder at 100°C by the Bragg's angle position in the intervals (a) 21° to 37° and (b) 48° to 54°.

Tf = 446.26°C (see Fig. 5), reported in Table 1. The corresponding specific heat capacity at these temperatures was found to be $C_P = -6.61\,\mathrm{J.g^{-1}{}^{\circ}C^{-1}}$ and $C_P = -0.22\,\mathrm{J.g^{-1}{}^{\circ}C^{-1}}$, respectively. Additionally, the fusion (ΔH_f) and crystallization (ΔH_c) enthalpies for these temperature ranges are also provided in Table 1.

Therefore, the effects of room temperature, 100°C and 400°C, were studied to observe the optimal temperature for the best formation of nanosized mesoporous hydroxyapatite powder. Compared with FTIR results, the effect of temperature at 100°C was found to be more effective for the nanosized mesoporous hydroxyapatite powder formation. In this study, the DSC results show decreases in both melting enthalpy and crystallization enthalpy with increasing calcination temperature. Therefore, in this observation, while it might initially seem counterintuitive that as temperatures increase from 100°C to 400°C, this is typically associated with increased crystallinity, there are several plausible explanations for this trend: first, that there is thermal decomposition or partial dehydroxylation (-OH); second, that there occured a reduction in organic residues; and third, the possiblity of crystallite growth and structural densification like nanocrystalline domains that

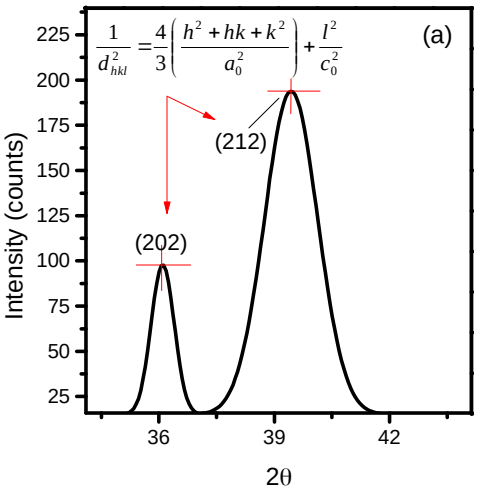

Figure 9: XRD patterns of nanosized mesoporous hydroxyapatite powder at 400°C by the Bragg's angle position in the intervals (a) 34° to 42° and (b) 55° to 62°.

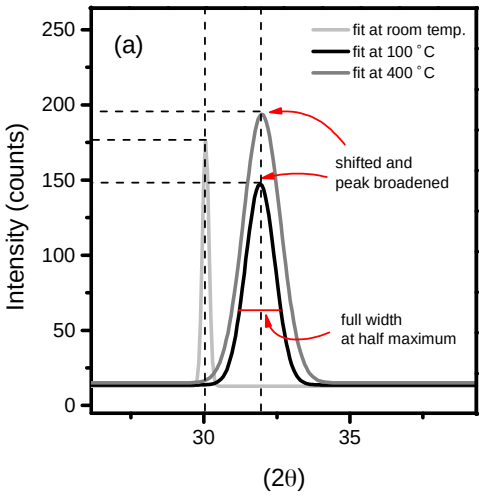

Figure 10: The Gaussian fit for the XRD pattern of nanosized mesoporous hydroxyapatite powder with respect to Bragg's angle 2θ in the ranges: (a) 26° to 35°, (b) 28° to 40°.

may grow into larger, more perfect crystals. In the meantime, the mass reduction has been showed by the TGA result (see Fig. 5). This indicates that organic residues were removed by the calcination temperature and then only nano-sized mesoporous hydroxyapatite powder is formed with slight impurities.

This is because the hydroxyl functional group (–OH) in the powdered nanosized mesoporous hydroxyapatite powder was detected more strongly at 100°C than at the other temperatures, as indicated by the vibration frequencies observed.

Table 1: Thermal quantities of powdered nano-sized mesoporous hydroxyapatite powder

T_i (°C)	T_f (°C)	ΔH_f (J/g)	ΔH_C (J/g)	C_p (J/(g °C))
143.24	233.87	118.14	24.23	- 6.61
361.04	446.26	61.85	15.16	- 0.22

iii XRD Results and discussions

The hexagonal crystal structure of nanosized mesoporous hydroxyapatite powder refers to the specific arrangement of atoms, ions or molecules in the crystal lattice that forms a hexagonal pattern. This arrange-

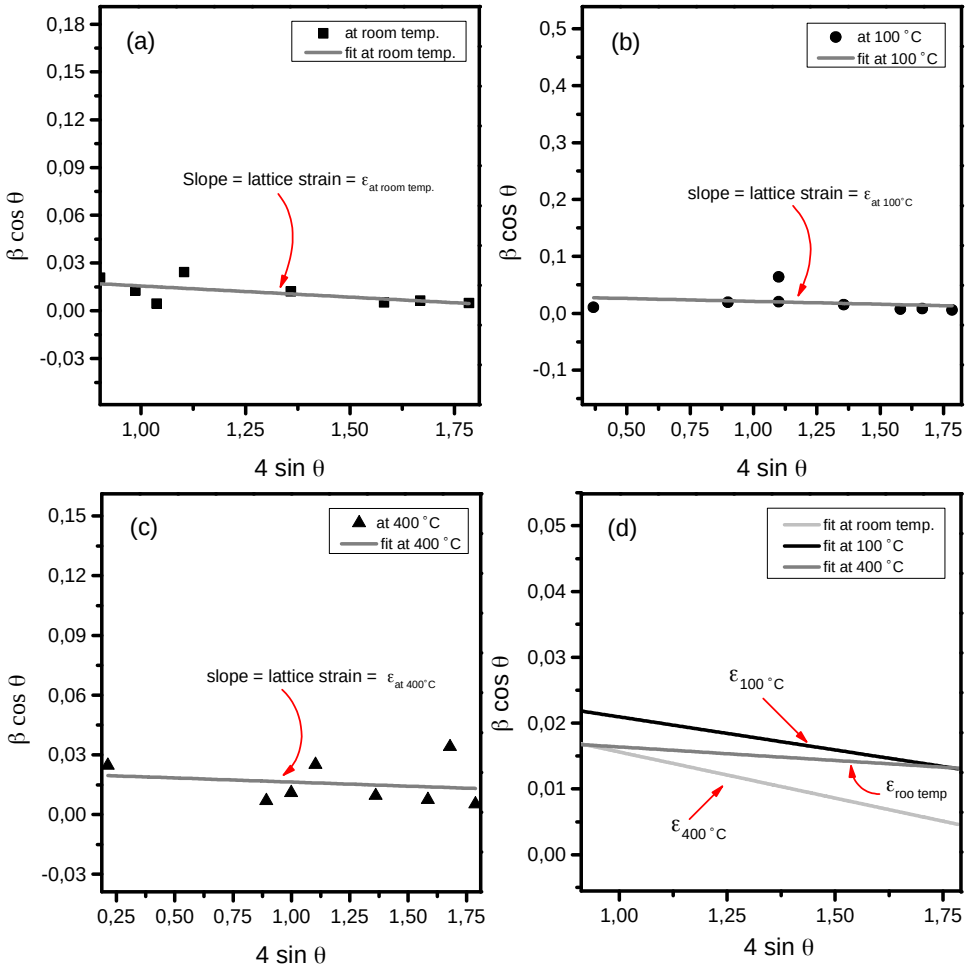

Figure 11: The Williamson-Hall plot method to define the crystallite size and microstrain quantities of nanosized mesoporous hydroxyapatite powder

ment was analyzed using XRD, where these patterns describe the specific angles and spacing of the crystal lattice planes in the hexagonal unit cell. The XRD spectrum peaks are simultaneously used to identify the spacing between planes in the lattice, which helps to confirm the hexagonal arrangement. The hexagonal crystal structure of the nanosized mesoporous hydroxyapatite powder was defined by lattice constants of $a_0 \approx b_0 \approx 9.416$ Å and $c_0 \approx 0$ (see Fig. 6).

In this study, several formulations were used to analyze the XRD patterns. First, Bragg's law, as shown in Eq. (1), was applied. Second, the hexagonal system was correlated with the Miller indices and the interplanar distance, as shown in Eq. (2). The Debye-Scherrer equation was used to calculate the crystallite size (d) from the broadening of the diffraction peaks (β), as shown in Eq. (3). The Williamson-Hall (W-H) plot method was then used to quantitatively analyze and separate the two factors contributing to the peak broadening in X-ray diffraction, as shown in Eq. (4). Both Eq. (4) and Eq. (5) were used to determine the lattice strain (ϵ) and dislocation density (δ). The percentage of crystallinity (Cr(%)) of nanosized mesoporous hydroxyapatite powder was calculated using Eq. (6). The results for ϵ, δ, and Cr(%) are shown in Table 2.

$$2d_{hkl}\sin(\theta) = n\lambda. \tag{1}$$

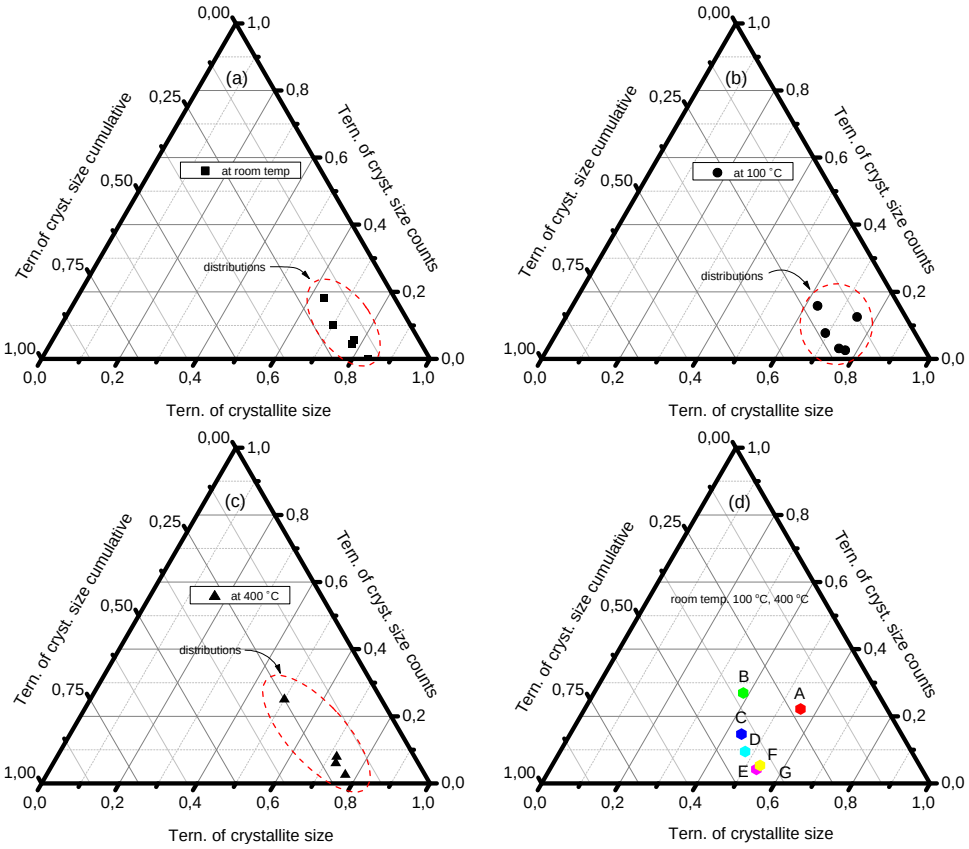

Figure 12: Ternary plot of crystallite size of nanosized mesoporous hydroxyapatite powder; (a) room temperature, (b) 100°C, (c) 400°C, and (d) all temperature

$$\frac{1}{d_{hkl}^2} = \frac{4}{3}\left(\frac{h^2+k^2}{a^2}\right) + \frac{l^2}{c^2}. \tag{2}$$

$$\frac{1}{d_{hkl}^2} = \frac{k\lambda}{\beta\cos(\theta)}. \tag{3}$$

$$\beta = \frac{k\lambda}{d\cos(\theta)} + 4\epsilon\tan(\theta). \tag{4}$$

$$\delta = \frac{1}{D^2}. \tag{5}$$

$$Cr(\%) = \frac{\text{Crys. Area}}{\text{Crys. Area} + \text{Amorp. Area}} \times 100. \tag{6}$$

Some results were found when some equations were used to describe the X-ray diffraction patterns in the particular Bragg's angle positions and derived by using the Eq. (1). The Miller indices of the hexagonal crystal structure of nanosized mesoporous hydroxyapatite powder are found to define the crystal planes in the unit cell using Eq. (2), and to understand its crucial interaction diffraction data of the XRD experiment. Particular Miller indices of the XRD patterns are shown: see Fig. 7, Fig. 8, and Fig. 9. Meanwhile, Eq. (3) to Eq. (6) are used to determine crystallite size, lattice strain (ϵ), dislocation density (δ), and percentage of crystallinity (Cr(%)) of the nanosized mesoporous hydroxyapatite powder. The Miller indices specific to nano-sized mesoporous hydroxyapatite powder at room temperature generated the following values: (002), (102), (201), (203), and (222) (see Fig. 7). Meanwhile, (002), (112), (222), and (320) are Miller indices values for nano-sized mesoporous hydroxyapatite powder at 100°C (see Fig. 8). Likewise, the Miller indices values at 400°C were described as: (202), (212), and

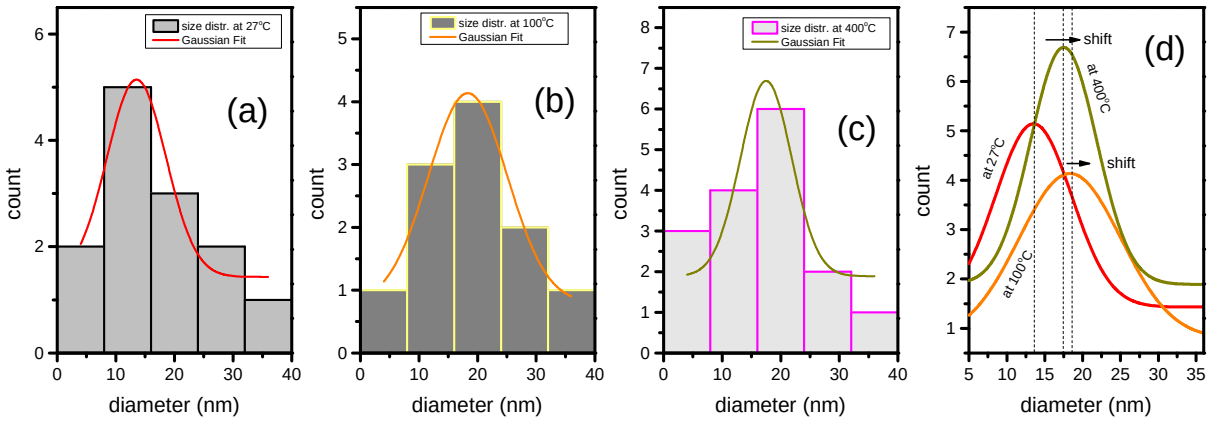

Figure 13: Crystallite size distribution of nanosized mesoporous hydroxyapatite powder at various temperatures; (a) room temperature, (b) 100°C, (c) 400°C, and (d) the combined curves for all various temperatures uses

(322) (see Fig. 9). Subsequently, the lattice constant or lattice parameter that is expressed in Eq. (2) was found using this formulation, with the results of a0 = b0 = 9.42 oA and c0 = 5.878 oA.

The broadening of the XRD peaks provides information on the Full Width at Half Maximum (FWHM) (see Fig. 10). Meanwhile, the crystallite size, lattice strain (ϵ), dislocation density (δ), and percentage of crystallinity (Cr(%)) of the nanosized mesoporous hydroxyapatite powder are presented (see Fig. 11 and Table 2). Particularly, the crystallinity at room temperature is approximately 72.28%, at 100°C it is about 68.93%, and it drops to around 62.46% at 400°C. However, these temperature effects do not seem to remove the impurities on all samples, which may have disrupted their microstructure, and this matter may be preventing nanosized mesoporous hydroxyapatite powder from achieving long-range order.

However, the crystallite size of nanosized mesoporous hydroxyapatite powder at various temperatures, conducted at room temperature, 100°C, and 400°C (see Fig. 12) has been determined. The ranges are detailed as follows: 3.0 nm – 6.0 nm ≈ 1; 9.0 nm – 12.0 nm ≈ 3; 15.0 nm – 18.0 nm ≈ 2; 21.0 nm – 24.0 nm ≈ 1; and 27.0 nm – 30.0 nm ≈ 1. Similarly, at 400°C, the ranges are as follows: 3.0 nm – 6.0 nm ≈ 3; 9.0 nm – 12.0 nm ≈ 0; 15.0 nm – 18.0 nm ≈ 2; 21.0 nm – 24.0 nm ≈ 2; and 27.0 nm – 30.0 nm ≈ 1.

The crystallinity of nanosized mesoporous hydroxyapatite powder was calculated using the formula in Eq. (6). This was used to assess the degree of structural order of solid materials like nanosized mesoporous hydroxyapatite powder. However, when the crystallinity is low, the structure tends to shift toward short-range order, or it tends to become amorphous. Conversely, when the crystallinity is high, the structure extends to long-range order, indicating that it became crystalline.

Meanwhile, the crystallite size distribution of nanosized mesoporous hydroxyapatite powder for all temperatures used in this effort shows that the majority fall within the range of 7.5 nm to 10.0 nm, as shown in Fig. 12 (d). These crystallite size values described

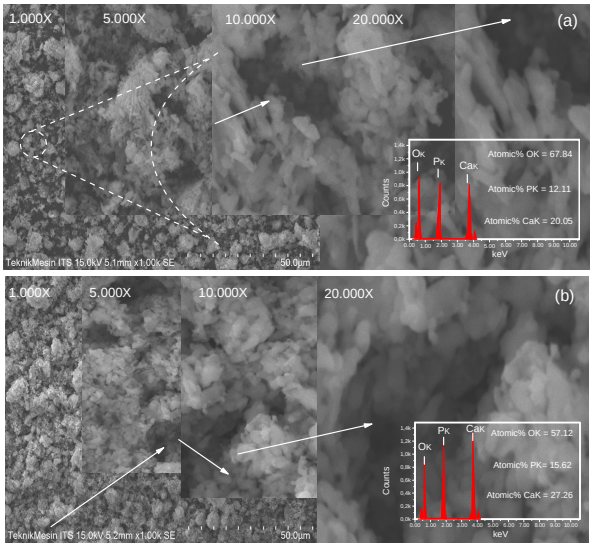

Figure 14: SEM-EDX images showing the surface morphology of nanosized mesoporous hydroxyapatite powder at (a) 100°C and (b) 400°C.

in the distributions were determined using the Debye-Scherrer equation, as shown in Eq. (2). Separately described are the crystallite size distributions: see Fig. 13 at room temperature, Fig. 13(b) at 100°C, Fig. 13(c), and Fig. 13(d) for comparison curves of the whole. The distribution peaks of curve were shifted when temperature increase is conducted in this effort, from room temperature to 100°C and then more increase to 400°C, which was previously determined using the Gaussian method, as shown in Fig. 13(d).

iv SEM-EDX Results and discussions

In this SEM-EDX test, two nanosized mesoporous hydroxyapatite powder samples were compared at 100°C and 400°C, where both showed distinct differences in the quantities of the hydroxyl group, as observed in previous FTIR and DSC-TG analyses. Therefore, these temperatures are preferred in the SEM-EDX test, and both are comparable in the test of the study of the surface morphology, as shown in Fig. 13. Subsequently, the Ca/P atomic ratios of these samples at 100°C and 400°C are approximately 1.63 and 1.73, respectively, as shown in Table 4. Both are close to the Ca/P [28–30] of the pure hydroxyapatite compound, which is 1.66 or 1.67.

The vibration of the hydroxyl group (OH) with a strong frequency occurred in a sample of nano-sized mesoporous hydroxyapatite powder at 100°C. Meanwhile, the vibrational bands associated with the P=O, P–O–P, and PO_4^{3-} groups shift to lower frequencies at 400°C. This observation is further confirmed by the EDX analysis, as shown in the inset picture in Fig. 14(a) and Fig. 14(b).

IV Conclusions

In this study, the effects of room temperature, 100°C, and 400°C on the microstructure of nanosized mesoporous hydroxyapatite powder were investigated. XRD analysis revealed that the crystalline structure exhibits a hexagonal phase. This finding is supported by the evaluation of key structural parameters such as crystallite size, microstrain, and lattice constants, which are consistent with a hexagonal structure with a face-centered cubic unit cell arrangement (FCC). Similarly, FTIR and SEM-EDX tests show the consistency of the functional group and the Ca/P atomic ratio of nanosized mesoporous hydroxyapatite powder, confirming that the material exhibits a nanoscale structure. Furthermore, the effect on its thermal properties was conducted using the DSC-TG, which involves the study of multiple thermal characteristics, such as their enthalpy of exothermic and endothermic processes, phase transitions from crystalline to molten phases, and specific heat capacity, which are indications of refractory materials, such as ceramics.

Table 2: Thermal quantities of powdered nanosized mesoporous hydroxyapatite powder

T (°C)	D (nm)	$(\epsilon \pm \Delta\epsilon)$	δ (nm^2)
room	4.68	- 0.014 $\pm$ 0.071	0.045
100	4.47	- 0.011 $\pm$ 0.016	0.049
400	6.79	- 0.004 $\pm$ 0.008	0.021

Table 3: Thermal quantities of powdered nanosized mesoporous hydroxyapatite powder

T (°C)	Element	Weight	Atomic	Ca/P
100	O	46.26	67.99	1.63
	P	17.86	12.15	
	C	35.88	19.86	
400	O	34.35	55.26	1.73
	P	19.59	16.16	
	Ca	46.06	28.58	

Acknowledgements - The authors would like to express their sincere gratitude to the Faculty of Science and Technology, Airlangga University, for their invaluable support and encouragement throughout this research, which was conducted under the university's outstanding basic research program, with the number of ID: 1665/UN3.FST/PT.01.03/2024.

[1] S. Sebastiammal et al., *Synthesis and characterisation of magnesium-wrapped hydroxyapatite nanomaterials for biomedical applications*, Surf. Interfaces, **44**, 103779 (2024).

[2] A. Mathirat et al., *Remineralizing Potential of Natural Nano-Hydroxyapatite Obtained from Epinephelus chlorostigma in Artificially Induced*

Early Enamel Lesion: An In Vitro Study, Nanomaterials, **12**, 22 (2022).

[3] A. Procopio et al., *Chemical Fingerprint of Zn-Hydroxyapatite in the Early Stages of Osteogenic Differentiation*, ACS Cent. Sci., **5**, 8 (2022).

[4] M. Harja, G. Ciobanu, *Studies on adsorption of oxytetracycline from aqueous solutions onto hydroxyapatite*, Sci. Total Environ., **628–629**, (2018).

[5] A. Biedrzycka, E. Skwarek, U. M. Hanna, *Hydroxyapatite with magnetic core: Synthesis methods, properties, adsorption and medical applications*, Adv. Colloid Interface Sci., **291**, 102401 (2021).

[6] M. Baladi et al., *Green sol–gel synthesis of hydroxyapatite nanoparticles using lemon extract as capping agent and investigation of its anticancer activity against human cancer cell lines (T98, and SHSY5)*, Arab. J. Chem., **16**, 4 (2023).

[7] B. H. Fellah, P. Layrolle, *Sol-gel synthesis and characterization of macroporous calcium phosphate bioceramics containing microporosity*, Acta Biomater., **5**, 2 (2009).

[8] I. Rutkowska, J. Marchewka, P. Jeleń, et al., *Chemical and Structural Characterization of Amorphous and Crystalline Alumina Obtained by Alternative Sol–Gel Preparation Routes*, Materials, **14**, 7 (2021).

[9] M. M. Pereira, A. E. Clark, L. L. Hench, *Calcium phosphate formation on sol-gel-derived bioactive glasses in vitro*, J. Biomed. Mater. Res., **28**, 6 (1994).

[10] K. P. Sanosh, M. C. Chu, A. Balakrishnan, et al., *Sol-gel synthesis of pure nano sized β-tricalcium phosphate crystalline powders*, Curr. Appl. Phys., **10**, 1 (2010).

[11] J. Livage, M. Henry, C. Sanchez, *Sol-gel chemistry of transition metal oxides*, Prog. Solid State Chem., **18**, 4 (1988).

[12] J. Livage, M. Henry, C. Sanchez, et al., *Chemical modification of alkoxide precursors*, J. Non-Cryst. Solids, **100**, 1-3 (1988).

[13] J. Schmitt, H. C. Flemming, *FTIR-spectroscopy in microbial and material analysis*, Int. Biodeterior. Biodegrad., **41**, 1 (1998).

[14] D. Naumann, V. Fijala, H. Labischinski, et al., *The rapid differentiation and identification of pathogenic bacteria using Fourier transform infrared spectroscopic and multivariate statistical analysis*, J. Mol. Struct., **174**, (1988).

[15] A. S. Posner, F. Betts, N. C. Blumenthal, *Formation and structure of synthetic and bone hydroxyapatites*, Prog. Cryst. Growth Charact., **3**, 1 (1980).

[16] H. H. Ram, J. Patel, S. Patel, et al., *Thermogravimetric analysis (TGA) and Differential scanning calorimetry (DSC) of some synthesized metal nanoparticles*, J. Sci. Healthc. Explor., **6**, 12 (2024).

[17] L. Müller, G. Rubio-Pérez, A. Bach, et al., *Consistent DSC and TGA Methodology as Basis for the Measurement and Comparison of Thermo-Physical Properties of Phase Change Materials*, Materials, **13**, 20 (2020).

[18] J. Sai Revanth, V. Sai Madhav, Y. Kalyan Sai, et al., *TGA and DSC analysis of vinyl ester reinforced by Vetiveria zizanioides, jute and glass fiber*, Mater. Today: Proc., **26**, 2 (2020).

[19] A. Naganthran, G. Verasoundarapandian, F. E. Khalid, et al., *Synthesis, Characterization and Biomedical Application of Silver Nanoparticles*, Materials, **15**, 2 (2022).

[20] N. T. Phuong, N. T. Thom, Pham T. Nam, et al., *Co2+ and Cr3+ ions removal from wastewater by using nanostructural hydroxyapatite*, Vietnam J. Chem., **60**, (2022).

[21] I. R. Gibson , I. Rehman, S. M. Best, et al., *Characterization of the transformation from calcium-deficient apatite to beta-tricalcium phosphate*, J. Mater. Sci. Mater. Med., **12**, 11 (2000).

[22] I. Irfan, M. K. Racik, S. Anand, *Microstructural evaluation of CoAl2O4 nanoparticles by Williamson–Hall and size–strain plot methods*, J. Asian Ceram. Soc., **6**, 1 (2018).

[23] D. Kumar, N. K. Verma, C. B. Singh, et al., *Crystallite size strain analysis of nanocrystalline*

La0.7Sr0.3MnO3 perovskite by Williamson-Hall plot method, AIP Conf. Proc., **1942**, 1 (2018).

[24] Y. T. Prabhu, K. V. Rao, B. S. Kumari, et al., *Synthesis of Fe3O4 nanoparticles and its antibacterial application*, International Nano Letters, **2**, 5 (2015).

[25] U. Holzwarth, N. Gibson, *The Scherrer equation versus the 'Debye-Scherrer equation'*, Nat. Nanotechnol., **9**, 6 (2011).

[26] P. Kibasomba, M. S. Dhlamini, M. Maaza, et al., *Strain and grain size of TiO 2 nanoparticles from TEM, Raman spectroscopy and XRD: The revisiting of the Williamson-Hall plot method*, Results Phys., **8**, 9 (2018).

[27] D. Brazete, P. M. C. Torres, J. C. C. Abrantes, et al., *Influence of the Ca/P ratio and cooling rate on the allotropic $\alpha \leftrightarrow \beta$-tricalcium phosphate phase transformations*, Ceram. Int., **44**, 7 (2018).

[28] M. Maciejewski, T. J. Brunner, S. F. Loher, et al., *Phase transitions in amorphous calcium phosphates with different Ca/P ratios*, Thermochim. Acta, **468**, 1-2 (2008).

[29] N. L. Davison, A. L. Gamblin, P. Layrolle, et al., *Liposomal clodronate inhibition of osteoclastogenesis and osteoinduction by submicrostructured beta-tricalcium phosphate*, Biomaterials, **19**, 35 (2014).

[30] N. L. Davison, X. Luo, T. Schoenmaker, et al., *Submicron-scale surface architecture of tricalcium phosphate directs osteogenesis in vitro and in vivo*, Eur. Cell. Mater., **27**, (2014).

[31] D. Le Nihouannen, D. Daculsi, A. Saffarzadeh , et al., *Ectopic bone formation by microporous calcium phosphate ceramic particles in sheep muscles*, Bone, **36**, 6 (2005).

[32] O. M. Omar, C. Granéli, K. Ekström, et al., *The stimulation of an osteogenic response by classical monocyte activation*, Biomaterials, **32**, 32 (2011).

[33] H. Yuan, J. D. De Bruijn, Y. Li, J. Feng, et al., *Bone formation induced by calcium phosphate ceramics in soft tissue of dogs: a comparative study between porous alpha-TCP and beta-TCP*, J. Mater. Sci. Mater. Med., **12**, 1 (2001).

[34] H. Yuan, K. Kurashina, J. D. de Bruijn, et al., *A preliminary study on osteoinduction of two kinds of calcium phosphate ceramics*, Biomaterials, **19**, 20 (1999).

[35] H. Yuan, Z. Yang, Y. Li, et al., *The stimulation of an osteogenic response by classical monocyte activation*, J. Mater. Sci. Mater. Med., **12**, 9 (1998).